Spectral features, electric properties, NBO analysis and reactivity descriptors of 2-(2-Benzothiazolylthio)-Ethanol: Combined experimental and DFT studies

ARTICLE *in* SPECTROCHIMICA ACTA PART A MOLECULAR AND BIOMOLECULAR SPECTROSCOPY · SEPTEMBER 2014

Impact Factor: 2.35 · DOI: 10.1016/j.saa.2014.09.091 · Source: PubMed

7 AUTHORS, INCLUDING:

Sinha Leena

University of Lucknow

74 PUBLICATIONS **308** CITATIONS

SEE PROFILE

Mehmet Karabacak

Celal Bayar Üniversitesi

131 PUBLICATIONS **1,488** CITATIONS

SEE PROFILE

Onkar Prasad

62 PUBLICATIONS **292** CITATIONS

SEE PROFILE

Abdullah M. Asiri

King Abdulaziz University

1,164 PUBLICATIONS **6,886** CITATIONS

SEE PROFILE

Spectrochimica Acta Part A: Molecular and Biomolecular Spectroscopy 136 (2015) 1205–1215

Contents lists available at ScienceDirect

Spectrochimica Acta Part A: Molecular and Biomolecular Spectroscopy

journal homepage: www.elsevier.com/locate/saa

Spectral features, electric properties, NBO analysis and reactivity descriptors of 2-(2-Benzothiazolylthio)-Ethanol: Combined experimental and DFT studies

Ruchi Srivastava [a], L. Sinha [a], M. Karabacak [b,*], O. Prasad [a], S.K. Pathak [a], A.M. Asiri [c,d], M. Cinar [e]

[a] Department of Physics, University of Lucknow, Lucknow, India
[b] Department of Mechatronics Engineering, H.F.T. Technology Faculty, Celal Bayar University, Turgutlu, Manisa, Turkey
[c] Department of Chemistry, Faculty of Science, King Abdulaziz University, Jeddah, Saudi Arabia
[d] Center of Excellence for Advanced Materials Research, King Abdulaziz University, Jeddah, Saudi Arabia
[e] Department of Science Education, Bayburt University, Bayburt, Turkey

HIGHLIGHTS

- Monomeric conformations of 2-(2-Benzothiazolylthio)-Ethanol were investigated.
- Spectroscopic properties of 2-(2-Benzothiazolylthio)-Ethanol were examined by FT-IR, FT-Raman, NMR and UV techniques.
- The vibrational frequencies, chemical shifts and electronic absorption wavelengths were calculated by DFT.
- A good agreement between the calculated and experimental wavenumbers is obtained.

GRAPHICAL ABSTRACT

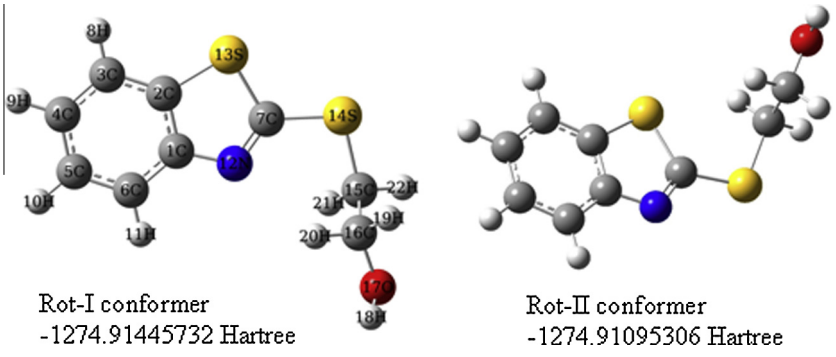

ARTICLE INFO

Article history:
Received 22 May 2014
Received in revised form 23 July 2014
Accepted 22 September 2014
Available online 30 September 2014

Keywords:
2-(2-benzothiazolylthio)-ethanol
FT-IR and FT-Raman spectra
NMR and UV spectra
NBO and NLO analysis
DFT

ABSTRACT

Quantum chemical calculations of ground state energy, geometrical structure and vibrational wavenumbers, nuclear magnetic behaviors, electronic absorption spectra along with the nonlinear optical properties of 2-(2-benzothiazolylthio)-ethanol (BTZTE) were carried out using density functional (DFT/B3LYP) method with 6-311++G(d,p) as basis set. The FT-IR and FT-Raman spectra were measured in the condensed state. The fundamental vibrational wavenumbers as well as their intensities were calculated, and a good correlation between experimental and scaled calculated wavenumbers was accomplished. The electric dipole moment, polarizability and the first hyperpolarizability values of the BTZTE were calculated at the same level of theory and basis set. The results show that the BTZTE molecule possesses nonlinear optical (NLO) behavior with non-zero values. Stability of the molecule arising from hyper-conjugative interactions and charge delocalization was analyzed using natural bond orbital (NBO) analysis. UV spectrum of the studied molecule was recorded in the region 200–500 nm and the electronic properties were predicted by time-dependent DFT approach. The calculated transition energies are in good concurrency with the experimental data. ^{1}H nuclear magnetic resonance (NMR) chemical shifts of the title molecule were calculated by the gauge independent atomic orbital (GIAO) method and compared with experimental results. The thermodynamic properties of the studied compound at different temperatures were calculated. Global and local reactivity descriptors were computed to predict reactivity and reactive sites on the molecule.

* Corresponding author. Tel.: +90 236 314 10 10; fax: +90 236 314 20 20.
E-mail address: mehmet.karabacak@cbu.edu.tr (M. Karabacak).

http://dx.doi.org/10.1016/j.saa.2014.09.091
1386-1425/

Introduction

The heterocyclic compounds containing nitrogen and sulphur belong to a class of compounds with recognized efficacy in medicinal chemistry. These compounds display broad spectrum of pharmacological activities and consequently have received special attention during past decades. Benzothiazole and its derivatives containing aromatic heterocyclic ring have attracted much attention of medicinal chemist due to their wide spectrum of biological properties which include anti-inflammatory, analgesic, antibacterial and antiviral activities [1–4]. Moreover it has been shown that the benzothiazole nucleus possesses a potent anticancer activity against human cancer [5–9]. It has been reported that benzothiazole derivatives own effective anticancer properties due to their structure being closely related to the naturally occurring purines as they can readily interact with biomolecules of the living systems [10]. Certain compounds containing the benzothiazole nucleus killed cells in a tumour-specific manner [11].

As the number of therapeutic agents synthesized with the help of benzothiazole nucleus is increasing day by day we feel that a complete investigation of this class of compounds is essential to have a deeper insight of the biological activities of this class. Present work in continuation to our earlier work on this class of compounds [12] deals with the molecular structure, electronic properties and vibrational spectra of 2(3H)-Benzothiazolone. To the best of our knowledge, neither quantum chemical calculations, nor the spectral analysis study of BTZTE has been reported yet. The FT-IR and FT-Raman spectra of the title compound were recorded and vibrational assignments were performed with the help of computed total energy distribution (TED). This work also comprises of the analysis of HOMO, LUMO and other molecular orbitals, 3-D Molecular Electrostatic Potential surface (MEPs) analysis along with calculation of electric moments to predict the NLO properties of the molecule. UV spectrum of the title molecule was also calculated and compared with the experimental spectrum. The transition energies calculated by TD-DFT results are in good agreement with the experimental data. NBO analysis of BTZTE were performed to reveal the information regarding charge transfer within the molecule. ^{1}H NMR chemical shifts of the molecule were calculated by GIAO method and compared with observed experimental ^{1}H NMR. The global reactivity descriptors such as chemical potential, electronegativity, hardness, softness, electrophilicity index and local reactivity descriptor like Fukui functions along with thermodynamical properties also have been computed to elaborate more characteristic properties of the title molecule.

Experimental details

The sample of the compound in solid state was purchased from Sigma–Aldrich Chemical Company (USA) with a stated purity of 98% and used as such for the spectroscopic measurements. FT-IR spectrum was recorded on a Bruker FT-IR spectrometer in the region 4000–400 cm^{-1}. KBr pellet of the solid sample was prepared from a mixture of KBr and the sample in 400:1 ratio using a hydraulic press. FT Raman spectrum in the range of 4000–100 cm^{-1} with a spectral resolution of 0.5 cm^{-1} was recorded on a Varian 7000 series spectrometer at AIRF. The 1064 nm laser line of Nd: YAG laser was used as the exciting wavelength. UV absorption spectra of BTZTE are recorded in methanol, ethanol, water and chloroform solvents, using Shimadzu 1800 UV–Vis recording spectrometer in the spectral region of 200–500 nm. ^{1}H NMR spectrum was recorded on Brucker DPX 300 MHz NMR spectrometer in DMSO-d_6 solvent with spectral band of 6009.615 Hz and acquisition time 5.4526 s.

Quantum chemical calculations

All calculations were carried out using Becke's three parameter hybrid exchange functional [13] with Lee–Yang-Parr correlation functional (B3LYP) [14,15] of DFT and 6-311++G(d,p) basis set [16]. The title molecule has two conformers corresponding the disposition of ethanol group with respect to the plane of the heterocyclic ring – Rot-I and Rot-II (Fig. 1). The geometry optimization and the energies associated with two possible conformers were computed. The computational results diagnose that the Rot-I is more stable. The lower value of ground state energy corresponding to first conformer tends it to be used for further quantum chemical calculations. Geometry optimization followed by calculation of the vibrational wavenumbers under the harmonic approximation were performed at DFT-B3LYP/6-311++G(d,p), and nonexistence of negative vibrational wavenumber confirm the stability of the corresponding lowest energy configuration leading to true minima. A scaling factor 0.983 up to 1700 cm^{-1} and 0.958 for greater than 1700 cm^{-1} was used to overcome the systematic errors caused by basis set incompleteness and vibrational anharmonicity [17]. The Raman and IR spectra were found to match well with the experimental spectra. The TED calculations (which show the relative contributions of the internal coordinates to each normal vibrational mode of molecule) were carried out by scaled quantum mechanics (SQM) method [18]. The vibrational assignments were carried out by combining the results of Gaussview 5.0.8 [19] and parallel quantum solutions (PQS) program [20].

The Raman intensities were calculated from the Raman activities (S_i) obtained with Gaussian 09 program, using the following relationship derived from the intensity theory of Raman scattering [21,22]

$$I_i = \frac{f(\upsilon_o - \upsilon_i)^4 S_i}{[\upsilon_i\{1 - \exp(-hc\upsilon_i/kT)\}]}$$

where υ_o is the wavenumber in cm^{-1} of the exciting light; υ_i is the vibrational wavenumber of the i^{th} normal mode; h, c and k are universal constants; f is a suitably chosen common normalisation factor for all peak intensities.

The calculated Raman and IR spectra were plotted using the pure Lorentzian band shape with a bandwidth of FWHM of 10 cm^{-1}. The components of the dipole moment, polarizability and first hyperpolarisability were also computed and then the total dipole moment (μ), mean polarizability $\langle\alpha\rangle$ and total first hyperpolarisability (β) [23,24] of the title compound were calculated by using Buckingham's definitions [25]. The α and β_{total} values of Gaussian output are in atomic units (a.u.) therefore they were converted into electrostatic units (esu) (for α; 1 a.u. = 0.1482 $\times$ 10^{-24} esu, for β; 1 a.u. = 8.6393 $\times$ 10^{-33} esu).

The electronic absorption spectrum requires calculation of the allowed excitations and oscillator strengths. The theoretical UV spectra were compared with the experimental spectra in solvated phase. The electronic properties such as Frontier molecular orbitals (FMOs) energies were also determined by time-dependent DFT method.

The NBO analysis [26] were performed in order to understand various second order interactions between the filled orbitals of one subsystem and vacant orbitals of another subsystem, which quantify the intermolecular delocalization or hyper conjugation. The second order perturbation theory analysis of Fock matrix in NBO basis of BTZTE was carried out to evaluate the donor–acceptor interactions. The interactions result in a loss of occupancy from the localized NBO of the idealized Lewis structure into an empty non-Lewis orbital. For each donor (i) and acceptor (j), the stabilization energy $E^{(2)}$ associated with the delocalization $i \rightarrow j$ is estimated as:

$$E^{(2)} = \Delta E_{ij} = q_i \frac{F(i,j)^2}{\varepsilon_j - \varepsilon_i}$$

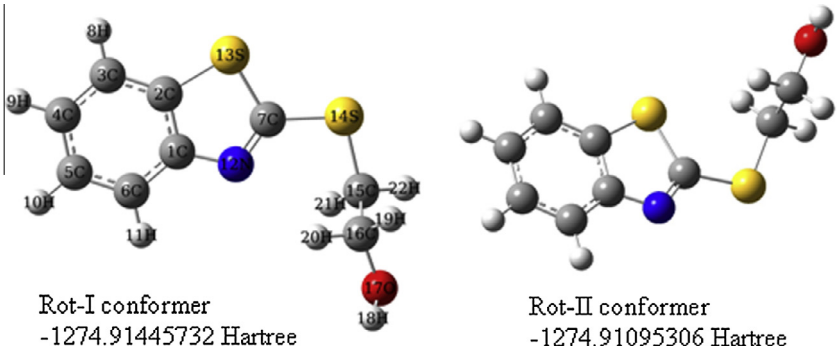

Fig. 1. The theoretically optimized two possible geometric structures of BTZTE at DFT-B3LYP/6-311++G(d,p) level of theory.

where q_i is the donor orbital occupancy, ε_i and ε_j are diagonal elements and $F(i,j)$ is the off diagonal NBO Fock matrix element. These calculations allow us to analyze the probable charge-transfers and the intermolecular bond paths. ^{1}H NMR chemical shifts for the title molecule are calculated with GIAO approach [27,28]. In addition, the changes in the thermodynamic functions such as heat capacity, entropy, and enthalpy were studied at various temperatures from the vibrational wavenumber calculations of BTZTE molecule.

Results and discussion

Molecular geometry

For BTZTE, two conformers are expected. These conformers are differs from one another by position of ethanol group with respect to the heterocyclic ring. The ground state energy of first conformer (Rot-I) is lower than Rot-II by 0.00350426 Hartree, inferring it to be more stable conformer, and its optimized parameters are collected in Table 1. In the optimized minimum energy structure of BTZTE, C15 atom of ethanol group is almost in the plane of the bicyclic ring with the dihedral angles C15—S14—C7—N12 and C15—S14—C7—S13 at −0.5° and −179.8°, respectively. The —C16H$_2$ group is almost perpendicular to the plane of the ring. The C—C bonds of the ring are found to vary in the range of 1.389–1.413 Å and the average value of the ring C—H bonds is 1.084 Å. The presence of N atom in the ring causes shortening of the adjacent C7—S13 bond in caparison to C15—S14, due to negative inductive (−I) effect.

Table 1
The optimized ground state structural parameters of BTZTE on DFT-B3LYP/6-311++G(d,p) level of theory.

Parameters	Values	Parameters	Values
Bond lengths	*(Å)*	*Bond angles*	*(°)*
C1—C2	1.413	C1—C6—C5	119.0
C1—C6	1.399	N12—C7—S13	116.0
C1—N12	1.388	N12—C7—S14	126.1
C2—C3	1.394	S13—C7—S14	117.9
C2—S13	1.758	C1—N12—C7	111.2
C3—C4	1.392	C2—S13—C7	88.1
C4—C5	1.402	C7—S13—C15	101.0
C5—C6	1.389	S14—C15—C16	113.2
C7—N12	1.289	S14—C15—H21	108.5
C7—S13	1.783	S14—C15—H22	104.6
C7—S14	1.762	C15—C16—O17	106.3
C15—S14	1.833	O17—C16—H19	110.8
C15—C16	1.522	O17—C16—H20	111.2
C16—O17	1.430	C16—O17—H18	108.9
O17—H18	0.962	CCH$_{\text{Ring average}}$	120.1
CH$_{\text{Ring average}}$	1.084	CCH$_{\text{Tail average}}$	110.2
CH$_{\text{Tail average}}$	1.093	HCH$_{\text{Tail average}}$	109.0
Bond angles	*(°)*	*Dihedral angles*	*(°)*
C2—C1—C6	119.5	C15—S14—C7—N12	−0.5
C2—C1—N12	115.3	C15—S14—C7—S13	−179.8
C6—C1—N12	125.2	O17—C16—C15—S14	−175.0
C1—C2—C3	121.6	H18—O17—C16—C15	−168.6
C1—C2—S13	109.3	C16—C15—S14—O17	5.5
C3—C2—S13	129.1	H18—O17—C16—H19	71.9
C2—C3—C4	118.0	C16—C15—S14—C7	−80.1
C3—C4—C5	120.9		
C4—C5—C6	120.9		

Vibrational analysis

In the present study, a satisfactory vibrational band assignment was ascertained for the title compound in terms of normal modes of vibration using FT-Raman, FT-IR spectroscopy and quantum chemical calculations. The optimized molecular conformation exhibits no special symmetries and consequently all the 60 vibrations from 3687 cm^{-1} to 32 cm^{-1} are both IR and Raman active. The assigned wavenumbers of the calculated vibrational modes along with their TED are given in Table 2. The calculated harmonic wavenumbers of BTZTE are usually higher than the corresponding experimental wavenumbers, this observed dissimilarity between theory and experiment could be a consequence of the anharmonicity and of the general tendency of quantum chemical methods to overestimate the force constants at the exact equilibrium geometry. The comparison of the scaled wavenumbers with experimental values reveals that the B3LYP method shows very good agreement with the experimentally observed spectra. The recorded experimental FT-IR and FT-Raman spectra of the title molecule along with corresponding simulated spectra are shown in Fig. 2. The vibrational analysis of BTZTE was discussed here under four heads: (i) phenyl ring vibrations (ii) fused thiazolyl ring vibrations (iii) bridge C—S vibrations (iv) ethanol group vibrations.

Phenyl ring vibrations

The phenyl ring spectral region predominantly involves the C—H, C—C, C=C stretching and C—C—C as well as C—C—H bending vibrations. The aromatic groups mostly have feeble sp^2 C—H stretching vibrations between 3000 and 3100 cm^{-1} while aliphatic C—H stretching appears just above 3000 cm^{-1} and sometimes overlap the aromatic C—H stretches [29,30]. The bands at 3077, 3050 and 3026 cm^{-1} in FT-IR and at 3052 and 3024 cm^{-1} in FT-Raman spectrum of BTZTE are assigned as C—H stretching mode of the ring which are in well agreement with the calculated scaled wavenumbers at 3064, 3058, 3048 and 3037 cm^{-1}. The vibrations involving C—H in-plane bending in aromatic compounds are found throughout in the region 1300–1000 cm^{-1}. The dominant C—H in-plane bending of the phenyl ring in present case are calculated at 1279, 1163 and 1124 cm^{-1} which well correlated with experimental bands at 1277/1277, 1160/1160 and 1131/1128 cm^{-1} in FT-IR/FT-Raman spectra, respectively. The C—H out of plane bending

Table 2
The recorded (FT-IR and FT-Raman) spectral data and computed vibrational wavenumbers along with the assignments of vibrational modes basing on TED results.

S. No.	Experimental		B3LYP/6-311++G(d,p)					Probable assignments &TED (⩾10%, given in parenthesis)
	FT-IR	FT-Raman	Unscaled	Scaled	I^{IR}	SA^{Raman}	I^{Raman}	
1	3415	–	3848	3687	42.07	158.83	0.01	νOH(100)
–	3306	3308	–	–	–	–	–	Overtone/Combination
2	3077	–	3198	3064	9.93	283.18	0.05	νCH_{ring} (99)
3	–	–	3192	3058	13.13	99.01	0.02	νCH_{ring} (100)
4	3050	3052	3181	3048	5.71	127.03	0.02	νCH_{ring} (100)
5	3026	3024	3170	3037	0.95	47.78	0.01	νCH_{ring} (100)
6	2991	2990	3138	3006	1.46	35.08	0.01	ν_{asym} C15—H_2 (99)
7	2940	2940	3076	2946	15.33	116.06	0.03	ν_{sym} C15—H_2 (89), ν_{asym} C16—H20(10)
8	–	2920	3060	2931	11.98	95.95	0.02	ν_{asym} C16—H_2 (87), ν_{sym} C15—H22(12)
9	–	2883	3005	2879	37.38	102.41	0.02	ν_{sym} C16—H_2 (100)
10	–	1586	1630	1603	3.52	41.93	0.06	νCC_{ring} (77)
11	1560	1560	1598	1570	2.37	30.61	0.05	νCC_{ring} (76)
12	–	–	1521	1495	18.08	37.12	0.07	ρC16—H_2 (77), ν C=N(10)
13	–	–	1513	1487	124.39	287.10	0.53	νC=N(62)
14	1456	1454	1485	1460	12.19	27.80	0.05	νCC_{ring} (82)
15	–	–	1464	1439	57.09	36.40	0.07	νCC_{ring} (62)
16	1430	1427	1459	1434	24.00	73.31	0.15	ρC15—H_2 (50)
17	1415	–	1438	1413	3.59	4.84	0.01	wC16—H_2 (50), ρC15—H_2 (24), βOH(12)
18	1312	1312	1342	1320	8.43	7.51	0.02	νCC_{ring} (77) (Kekule mode)
19	1286	–	1316	1294	0.85	14.48	0.04	tC(15,16)—H_2 (87)
20	1277	1277	1301	1279	10.33	64.93	0.18	βCH_{ring} (64), νC—N(14)
21	–	–	1291	1269	9.52	4.76	0.01	wC15—H_2 (70), βOH(18)
22	1240	1238	1260	1239	25.59	115.48	0.35	νC—N(33), βCH_{ring} (26), νCC_{ring} (21)
23	1215	–	1236	1215	25.21	5.18	0.02	βCH of C(15,16)—H_2 (52), βOH(27)
24	1186	1191	1208	1188	11.01	2.58	0.01	tC(15,16)—H_2 (61), βOH(22)
25	1160	1160	1183	1163	0.29	3.34	0.01	βCH_{ring} (92)
26	1131	1128	1143	1124	7.40	27.25	0.11	βCH_{ring} (46), νCC_{ring} (29)
27	1059	1057	1084	1065	11.44	13.34	0.06	βCCC_{ring} (23), νC2—S(22), νCC_{ring} (18)
28	1032	–	1048	1030	13.66	1.38	0.01	tC15—H_2 (45), rC16—H_2 (38)
29	–	–	1040	1022	10.64	17.94	0.09	νCC_{ring} (55)(RBM), βCH_{ring} (19), νC—O(11)
30	1018	1014	1039	1021	110.17	18.01	0.09	νC—O(81)
31	999	1001	1012	995	5.94	4.20	0.02	νCH_2—CH_2 (68), βOH(15)
32	–	–	991	974	177.23	29.46	0.16	ν_{asym} SCS(33), βNCS(13,14)(25), βCNC(14)
33	946	–	983	966	0.00	0.00	0.00	γCH_{ring} (85)
34	936	934	947	931	1.68	0.10	0.00	γCH_{ring} (89)
35	852	852	867	852	1.30	11.98	0.09	βCCC_{ring} (33), νCC_{ring} (18), νC—N(17), νC7-S(10)
36	824	825	859	844	0.91	0.03	0.00	γCH_{ring} (90)
37	762	760	773	760	5.44	2.71	0.03	rC(15,16)—H_2 (91)
38	–	–	763	750	61.95	1.01	0.01	γCH_{ring} (77)
39	729	732	739	727	26.63	11.21	0.12	νS—CH_2 (68), βCCO(12)
40	707	706	725	713	13.12	0.13	0.00	$\gamma CCCC_{ring}$ (57), γCH_{ring} (34)
41	690	–	713	701	3.75	16.64	0.20	Ring deformation (81)
42	658	656	665	653	15.12	2.27	0.03	νC7—S (47), βCCN(12)
43	598	598	606	596	1.85	4.68	0.08	Ring deformation (75)
44	583	–	594	584	0.40	0.20	0.00	γCCNC(37), $\gamma CCCC_{ring}$ (28), γCCNC (15)
45	–	–	526	517	0.15	0.17	0.00	γCCNC(48), $\gamma CCCC_{ring}$ (38)
46	480	502	507	498	0.11	11.23	0.29	βCCC_{ring} (20), νC2—S(17), βCCN(16), βCCS(12), βCSC(11)
47	430	442	435	427	4.73	0.02	0.00	$\gamma CCCC_{ring}$ (86)
48	407	405	424	417	5.84	2.13	0.08	βC—S14—C(20), ν_{asym} C—S13—C(15), βSC—N,S(15), βCCO(11)
49	–	366	388	381	7.13	3.29	0.15	ν_{asym} C—S14—C(29), βCCO(13)
50	–	331	362	356	5.73	0.91	0.05	ν_{sym} C—S14—C(25), βC—C—S13(17), βCCN(15), βCCC_{ring} (13)
51	–	303	292	287	0.36	0.74	0.06	Ring butterfly (75)
52	–	262	264	260	2.55	2.99	0.31	βC—S14—C(24), βCCO(21), βC—C—S14(17)
53	–	227	226	222	6.93	3.28	0.48	βC—C—S14(31), βC—S14—C(22), rC16—H_2 (19)
54	–	208	190	187	31.26	1.07	0.23	γCCSC(35), γOH(31), γCCCC(14)
55	–	183	185	182	78.47	1.21	0.27	γOH(60), γCCSC(15)
56	–	151	154	151	0.60	0.57	0.19	rC15—H_2 (28), βS—C—S(24), βN—C—S14(22)
57	–	–	107	105	9.24	0.45	0.31	Ring butterfly (80)
58	–	–	84	83	12.22	0.90	1.00	rCH_2OH(78)
59	–	–	51	50	0.70	2.00	0.01	rCH_2OH(65), βC—S14—C(17), βS—C—S,N(11)
60	–	–	33	32	0.78	3.16	0.04	γNCS14C(98)

Abbreviation: ν_{sym}; symmetric stretching, ν_{asym}; asymmetric stretching, β; in-plane bending, γ; out-of-plane bending, ρ; scissoring, t; twisting, r; rocking, w; wagging. The out-of-plane banded atoms were underlined in the last column.
I^{IR} and I^{Raman}; IR and Raman Intensity (km mol^{-1}), SA^{Raman}; Raman scattering activity (A^4 amu^{-1}), wavenumbers are in (cm^{-1}).

modes is usually medium intensity and is observed in the region 950–600 cm^{-1} [30–33]. The C—H out of plane vibration in BTZTE are calculated to be nearly pure mode and the assigned wavenumbers for this mode are 946, 936 and 824 cm^{-1} in FT-IR and at 934 and 825 cm^{-1} in FT-Raman spectrum are well matched with theoretical values at 966, 931, 844 and 750 cm^{-1}. The interesting Kekule mode vibration of the phenyl ring in the title compound is assigned as a band at 1312/1312 in FT-IR/FT-Raman spectra with calculated wavenumber at 1320 cm^{-1}. From the visualisation of vibrations in Gaussview program and TED the vibration

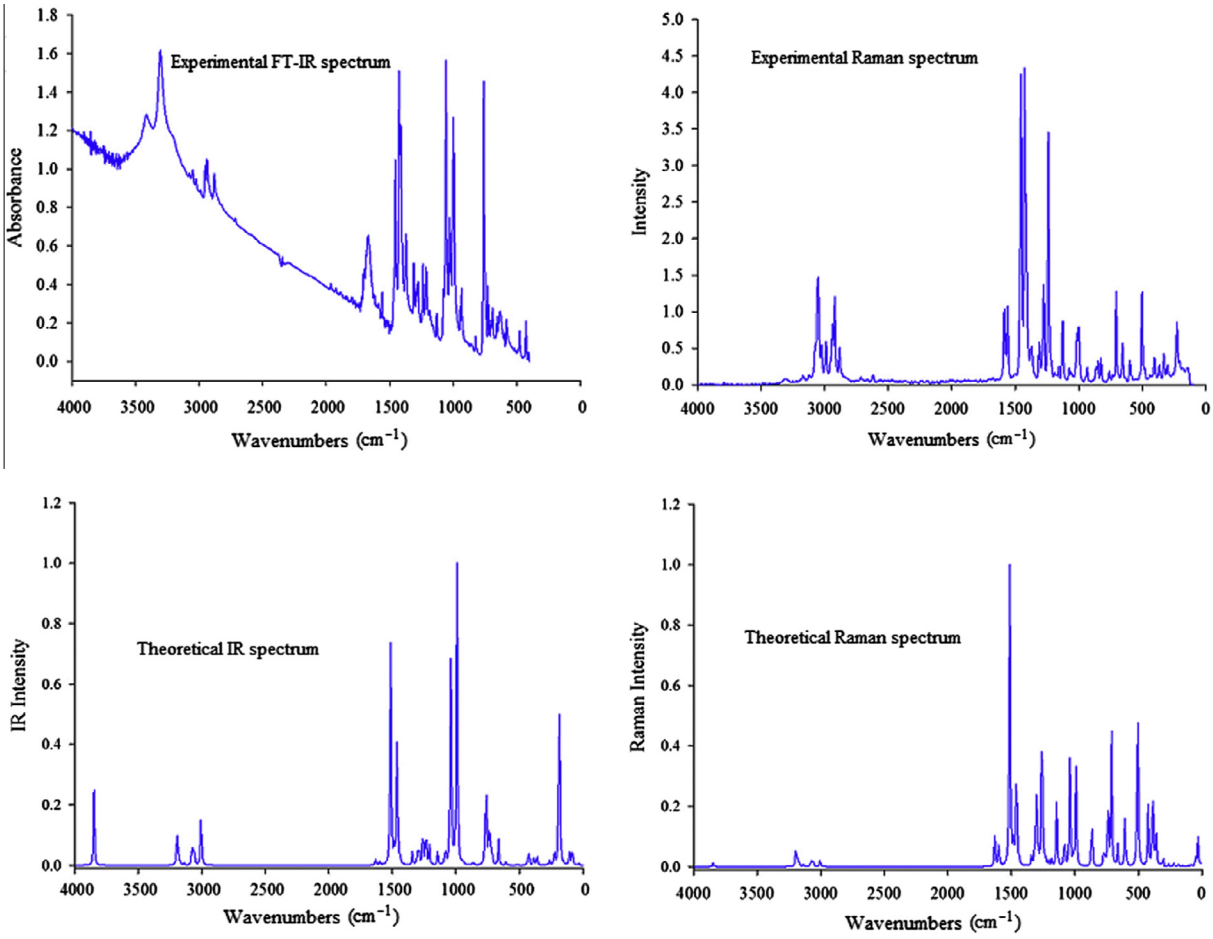

Fig. 2. Comparison of recorded FT-IR and FT-Raman spectra in solid state with simulated IR and Raman spectra of BTZTE.

corresponding to wavenumber 1022 cm^{-1} was assigned as ring breathing mode (RBM). This vibration is substituent sensitive and was reported at 1010 cm^{-1} in case of 2(3H)-Benzothiazolone [12].

The calculated wavenumbers corresponding to C—C stretching at 1603, 1570, 1460 and 1439 cm^{-1} are also in good agreement with experimental findings. The computed bands at 1065 and 852 cm^{-1} aroused due to the trigonal ring bending modes making 23% and 33% contribution to TED. The peaks at 690 and 598 cm^{-1} in FT-IR spectrum of BTZTE are due to ring deformation mode with theoretical predicted wavenumbers at 701 and 596 cm^{-1} having TED more than 75%. In the present case the interesting phenyl ring torsional mode (Puckering) is found at 713 cm^{-1} and is matched well with peaks at 707 and 706 cm^{-1} in FT-IR and FT-Raman spectra, respectively. The other dominant torsional vibration for the title molecule is assigned as a band at 430/442 cm^{-1} in FT-IR/FT-Raman spectra.

Fused thiazolyl ring vibrations

The title compound consists of a thiazolyl ring fused with the phenyl ring and hence bands associated with C—N, C═N, C—S stretching along with in plane bending, out of plane bending and torsion vibrations involving these bonds must appear in the spectrum of the BTZTE compound. The identification of C═N and C—N vibrations is difficult task since the mixing of several bands is possible in the region. The calculated scaled wavenumber at 1487 cm^{-1} is assigned to C═N stretching vibration and the band at 1240 and 1238 cm^{-1} in FT-IR and FT-Raman spectra, respectively is assigned to C—N stretching mode which is in good correlation with theoretical predicted wavenumber at 1239 cm^{-1}. We assigned the bands at 658/656 and 480/502 in FT-IR/FT-Raman spectra as C—S stretching mode of thiazolyl ring. The ring butterfly modes are calculated at 287 and 105 cm^{-1}.

Bridge C—S vibrations

The S atom connecting thiazolyl ring and ethanol group acts as a bridge. The stretching vibration assigned to the C—S linkage occurs in the region 700–600 cm^{-1} [34,35]. For 2(3H)-Benzothiazolone C—S stretching was calculated as mixed mode at 1112, 1042, 690 and 614 cm^{-1} [12]. In the present case the C—S stretching vibration of the ring is found in the range of 1065–417 cm^{-1}. The wavenumbers associated with C—S14—C asymmetric and symmetric stretching vibrations are calculated at much lower wavenumbers due to S14 being connected to heavy heterocyclic ring on one side and ethanol group on the other side. The calculated values for asymmetric and symmetric stretches at 381 and 356 cm^{-1} respectively are in good consensus with peaks observed at 366 and 331 cm^{-1} in FT-Raman spectrum. The band at 262 and 227 cm^{-1} in FT-Raman spectrum are dominant modes for C—S—C in plane bending vibrations mixed with CCO, CCS and CH_2 rocking modes.

Ethanol group vibrations

The vibrations associated with ethanol group are O—H stretching, in plane bending and out of plane bending along with CH_2 symmetric and asymmetric stretching, scissoring, twisting, rocking and wagging modes. The O—H stretching vibration is very sensitive to hydrogen bonding. A free hydroxyl group or a non-hydrogen bonded hydroxyl group absorbs in the range of 3700–3500 cm^{-1}. The intra-molecular hydrogen bonding present in the system

Table 3
Calculated molecular orbital energies (eV), energy differences between transition levels and in the ground state dipole moments (D) of isolated and solvated studied molecule.

	TD-B3LYP/6-311++G(d,p)				
Parameters	Gas	Chloroform	Ethanol	Methanol	Water
E_{total} (eV)	−34687.9245	−34692.3753	−34688.2108	−34688.2111	−34692.7125
E_{LUMO+3}	−0.3589	−0.2305	−0.2052	−0.2038	−0.2014
E_{LUMO+2}	−0.6542	−0.6191	−0.6169	−0.6169	−0.6166
E_{LUMO+1}	−0.7121	−0.7312	−7.5213	−0.7535	−0.7565
E_{LUMO}	−1.2691	−1.3075	−1.3339	−1.3358	−1.3394
E_{HOMO}	−6.2927	−6.3362	−6.3640	−6.3659	−6.3694
E_{HOMO-1}	−6.7501	−6.7819	−6.8059	−6.8078	−6.8111
$\Delta E_{(LUMO)-(HOMO-1)}$	**5.4810**	**5.4744**	**5.4720**	**5.4720**	**5.4717**
$\Delta E_{(LUMO)-(HOMO)}$	**5.0235**	**5.0287**	**5.0301**	**5.0301**	**5.0301**
$\Delta E_{(LUMO+3)-(HOMO)}$	**5.9338**	**6.1057**	**6.1588**	**6.1621**	**6.1681**
$\Delta E_{(LUMO+2)-(HOMO-1)}$	**6.0959**	**6.1628**	**6.1890**	**6.1909**	**6.1944**
$\Delta E_{(LUMO+2)-(HOMO)}$	**5.6385**	**5.7171**	**5.7471**	**5.7490**	**5.7528**
$\Delta E_{(LUMO+1)-(HOMO)}$	**5.5806**	**5.6050**	**−1.1573**	**5.6124**	**5.6129**
μ_x	0.9156	1.1433	1.2336	1.2393	1.2504
μ_y	0.5983	0.5204	0.4287	0.4213	0.4064
μ_z	1.3779	1.6378	1.7751	1.7849	1.8042
μ_{tot}	1.7592	2.0641	2.2037	2.2134	2.2324

HOMO is no 55.

reduces the hydroxyl stretching band to 3559–3200 cm^{-1} region [36,37]. In BTZTE, the OH group of ethanol in the solid state absorb broadly near 3450–3300 cm^{-1}. In the FT-IR spectra of BTZTE, the strong peak at 3415 cm^{-1} is therefore assigned to the OH stretching vibration, while the theoretical analysis predict this scaled wavenumber at 3687 cm^{-1} with 100% TED. The discrepancy between the theoretical and experimental wavenumber is justified owing to the O—H group vibration being the most sensitive to the environment, and illustrates marked shifts in the spectra of the hydrogen bonded species. The O—H in-plane bending vibration is found to spread over range 1413–995 cm^{-1} while the calculated scaled wavenumber 182 cm^{-1} is assigned as dominant mode of O—H out-of-plane bending and in good agreement with a band at 183 cm^{-1} in FT-Raman spectrum.

The calculated wavenumbers at 3006, 2946, 2931 and 2879 cm^{-1} are assigned to CH_2 stretching vibrations, well matched with bands at 2991, 2940 cm^{-1} in FT-IR and 2990, 2940, 2920 and 2883 cm^{-1} in FT-Raman. The CH_2 scissoring vibrations appear normally in the region 1490–1435 cm^{-1} as medium intense bands [38,39]. In the present case CH_2 scissoring vibrations are assigned scaled wavenumbers at 1495 (TED 77%) and at 1434 cm^{-1} (TED 50%) and wagging vibrations at 1413 and 1269 cm^{-1} (TED 50% and 70%) which are in good correlation with experimental findings. The band at 1186 and 1032 cm^{-1} in FT-IR spectrum of the title compound are assigned as dominant mode for CH_2 twisting vibrations. The remainder of the observed and calculated wavenumbers and their assignments for the present molecule are given in Table 2.

Electronics properties and UV spectral analysis

The frontier orbital's gap determines the way a molecule interacts with other species. The chemical reactivity and kinetic stability of a molecule largely depend on the energy gap between the highest occupied molecular orbital (HOMO) and the lowest unoccupied molecular orbital (LUMO). Lower the frontier orbital gap, softer and more polarisable is the molecule having high chemical-reactivity and low kinetic stability. In present study, the energies of frontier orbitals were computed in different solvents (Table 3), and the predicted shapes of FMOs are given in Fig. 3. Frontier orbital gap of BTZTE is found to be 5.0235 eV in gas phase and slightly higher in different solvents. HOMO is distributed uniformly almost over the phenyl and heterocyclic rings having bonding character while LUMO is found to be spread over the atoms in both ring and reflects high anti-bonding nature. The nodes of HOMOs and LUMOs are almost placed symmetrically.

On the basis of a fully optimized ground state structure TD-DFT was used to find out the low lying excited states of BTZTE in gas phase as well as in methanol, ethanol, water and chloroform solvents. The calculated results involving the vertical excitation energies, oscillator strengths (*f*) and absorption wavelengths were carried out and compared with measured experimental data (Table 4). The recoded UV spectra of the title compound are shown in Fig. 4 while the theoretical spectra were provided in Fig. S1. By TD-DFT calculation one intense transition was predicted at 273.23 nm in gas phase. Experimental peaks in chloroform, ethanol, methanol, and water at 279.80, 280.00, 279.80 and 279.60 nm respectively are in well agreement with the theoretical ones and are assigned due to electronic transition from HOMO → LUMO. The most intense peak observed at 222.00, 223.07, 222.80 and 223.20 nm in chloroform, ethanol, methanol and water respectively are assigned due to transition from HOMO → LUMO + 1 in good correlation with corresponding predicted values. Some other theoretical wavelengths corresponding to electronic transitions are given in Table 4 along with observed experimental values.

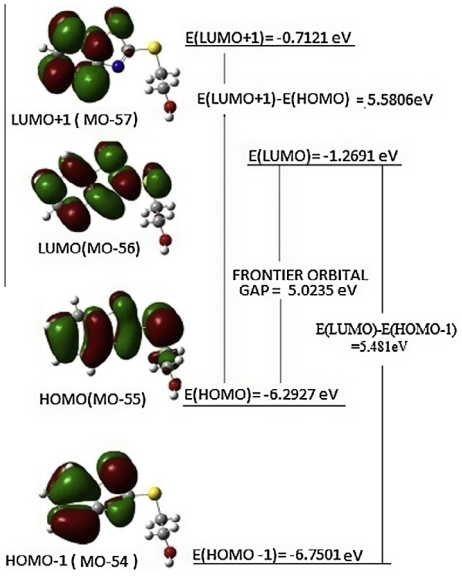

Fig. 3. Patterns of the HOMO, LUMO and other significant molecular orbitals of BTZTE obtained with TD-DFT-B3LYP/6-311++G(d,p) method.

Table 4
The calculated and experimental absorption wavelengths (λ, nm), excitation energies (E, eV), and absorbance values or oscillator strengths (f) of the investigated compound.

Experimental			TD-B3LYP/6-311++G(d,p)		
λ (nm)	E (eV)	Abs.	λ (nm)	E (eV)	f
			Gas		
			273.23 (55 → 56)	4.5377	0.2332
			265.33 (55 → 57)	4.6728	0.1007
			262.51 (55 → 58)	4.7231	0.0089
			240.25 (54 → 58)	5.1605	0.0001
			236.76 (55 → 57)	5.2368	0.0916
			234.44 (55 → 59)	5.2885	0.0139
			Chloroform		
279.80	4.4312	1.014	276.80 (55 → 56)	4.4793	0.3868
288.60	4.2960	0.926	266.18 (54 → 56)	4.6580	0.0870
			259.48 (55 → 58)	4.7782	0.0020
222.00	5.5849	1.610	238.30 (55 → 57)	5.2029	0.1565
			237.70 (54 → 58)	5.2160	0.0159
			229.85 (55 → 59)	5.3942	0.0033
			Ethanol		
280.00	4.4280	1.581	276.17 (55 → 56)	4.4893	0.3631
			265.87 (54 → 56)	4.6633	0.0897
			258.02 (55 → 58)	4.8052	0.0017
223.07	5.5581	2.079	237.77 (55 → 57)	5.2144	0.1582
			236.45 (54 → 58)	5.2436	0.0034
			228.35 (55 → 59)	5.4296	0.0036
			Methanol		
279.80	4.4312	0.625	275.93 (55 → 56)	4.4933	0.3538
288.80	4.2931	0.568	265.80 (54 → 56)	4.6646	0.0905
			257.92 (55 → 58)	4.8072	0.0017
222.80	5.5648	0.996	237.62 (55 → 57)	5.2178	0.1539
			236.34 (54 → 58)	5.2459	0.0036
			228.25 (55 → 59)	5.4319	0.0035
			Water		
279.60	4.4343	1.469	275.97 (55 → 56)	4.4927	0.355
288.80	4.2931	1.316	265.79 (54 → 56)	4.6648	0.0905
			257.73 (55 → 58)	4.8105	0.0016
223.20	5.5548	2.342	237.63 (55 → 57)	5.2176	0.1548
			236.19 (54 → 58)	5.2494	0.0029
			228.08 (55 → 59)	5.4359	0.0037

HOMO is no 55.

MEPs for BTZTE were plotted using B3LYP/6-311++G(d,p) level for the optimized geometry, to predict the reactive sites for electrophilic and nucleophilic shown in Fig. 5. The electron rich (red color) regions of MEPs are related to electrophilic activity and the electron poor (blue color) to the nucleophilic reactivity. As depicted[1] in Fig. 5, the possible sites for electrophilic attack in the title molecule are mainly over the carbon atoms of ring, S14, S13 and O17 while preferred sites for nucleophilic attack are mainly over the H18 and other H atoms of ethanol group.

Electric moments

To predict NLO behavior of BTZTE, the components of dipole moment, polarizability and hyperpolarizability were computed using DFT method. Dipole moment in a molecule is mainly used to study the intermolecular interactions involving the non-bonded type dipole–dipole interactions, can be represented as a vector in three dimensions which reflects the molecular charge distribution and consequently also can be used as descriptor to depict the charge movement across the molecule. Dipole moment of a molecule also depends on its environments, therefore various solvents (chloroform, ethanol, methanol and water) available in Gaussian software has been implemented and comparison of computed results (Table 3) shows that total dipole moment of BTZTE

[1] For interpretation of color in Fig. 5, the reader is referred to the web version of this article.

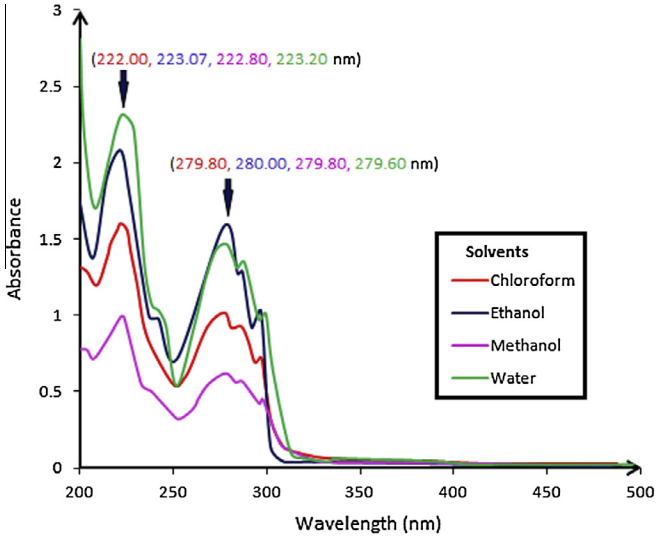

Fig. 4. Recorded UV-spectra of BTZTE in various solvents.

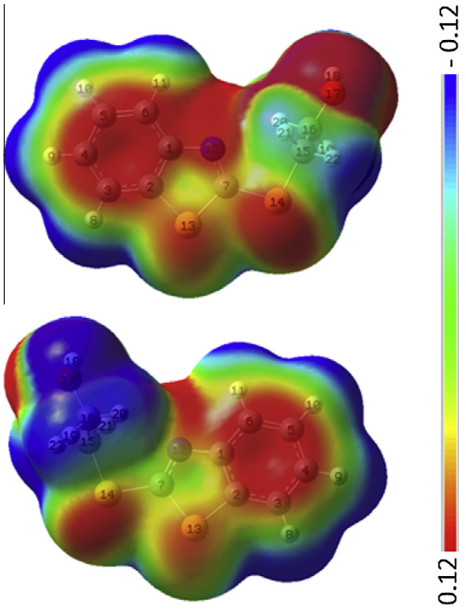

Fig. 5. MEPs for BTZTE calculated by B3LYP/6-311++G(d,p) method.

(1.7592 Debye in gas phase) increases with polar nature of solvents. Theoretical prediction of the electric polarizability and hyperpolarizability was done (Table 5) to arrive at the better understanding/description of the title molecule in absence of the experimental data. The mean polarizability and total first static hyperpolarizability (β_{total}) of the title molecule is found to be

Table 5
Polarizability and hyperpolarizability of BTZTE.

	a.u.	($\times 10^{-24}$) esu		a.u.	($\times 10^{-30}$) esu
α_{xx}	224.2646	33.2360	β_{xxx}	687.1029	5.9361
α_{xy}	16.0956	2.3854	β_{xxy}	162.2372	1.4016
α_{yy}	163.4767	24.2272	β_{xyy}	62.0523	0.5361
α_{xz}	7.2891	1.0802	β_{yyy}	−78.9079	−0.6817
α_{yz}	−5.9910	−0.8879	β_{xxz}	46.0676	0.3980
α_{zz}	95.1851	14.1064	β_{xyz}	2.3297	0.0201
α_{mean}	160.9755	23.8566	β_{yyz}	15.0748	0.1302
			β_{xzz}	9.3675	0.0809
			β_{yzz}	−41.0093	−0.3543
			β_{zzz}	33.4170	0.2887
			β_{tot}	765.5647	6.6139

Table 6
Second order perturbation theory analysis of Fock matrix in NBO basis for BTZTE.

Donor (*i*)	Type	ED/e	Acceptor (*j*)	Type	ED/e	$E^{(2)}$ kcal/mol	$E(j)$–$E(i)$ a.u.	$F(i,j)$ a.u.
C1—C2	σ	1.97123	C3	RY*(1)	0.00644	1.60	1.71	0.047
	σ		C6	RY*(1)	0.00551	1.01	1.98	0.040
	σ		C1—C6	σ*	0.02509	4.26	1.27	0.066
	σ		C1—N12	σ*	0.02640	1.14	1.16	0.033
	σ		C2—C3	σ*	0.02077	4.19	1.28	0.065
	σ		C3—H8	σ*	0.01474	2.38	1.14	0.047
	σ		C6—H11	σ*	0.01315	1.88	1.15	0.042
	π	1.63698	C3	RY*(3)	0.00113	2.20	0.99	0.046
	π		C6	RY*(3)	0.00078	1.07	0.76	0.028
	π		S13	RY*(1)	0.00391	2.46	0.90	0.046
	π		C3—C4	π*	0.32827	19.59	0.29	0.068
	π		C5—C6	π*	0.30984	16.30	0.30	0.063
	π		C7—N12	π*	0.38845	12.30	0.25	0.050
C1—C6	σ	1.97081	C5	RY*(1)	0.00590	1.16	1.80	0.041
	σ		C5	RY*(2)	0.00225	1.49	1.98	0.049
	σ		C1—C2	σ*	0.04158	4.68	1.24	0.068
	σ		C1—N12	σ*	0.02640	2.11	1.16	0.044
	σ		C2—S13	σ*	0.02635	2.90	0.90	0.046
	σ		C5—C6	σ*	0.01340	2.63	1.29	0.052
	σ		C5—H10	σ*	0.01281	2.21	1.15	0.045
	σ		C7—N12	σ*	0.02500	1.69	1.27	0.041
C1—N12	σ	1.97142	C7	RY*(1)	0.01014	1.17	1.47	0.037
	σ		C7	RY*(2)	0.00674	2.05	1.93	0.057
	σ		C1—C2	σ*	0.04158	1.41	1.31	0.039
	σ		C1—C6	σ*	0.02509	2.03	1.35	0.047
	σ		C2—C3	σ*	0.02077	1.94	1.35	0.046
	σ		C5—C6	σ*	0.01340	1.05	1.36	0.034
	σ		C7—N12	σ*	0.02500	1.73	1.35	0.043
	σ		C7—S14	σ*	0.04531	6.72	0.97	0.072
C2—C3	σ	1.97844	C4	RY*(1)	0.00610	1.05	1.84	0.039
	σ		C4	RY*(2)	0.00219	1.41	2.01	0.048
	σ		C1—C2	σ*	0.04158	4.06	1.26	0.064
	σ		C1—N12	σ*	0.02640	2.44	1.18	0.048
	σ		C3—C4	σ*	0.01539	2.94	1.31	0.055
	σ		C3—H8	σ*	0.01474	1.24	1.16	0.034
	σ		C4—H9	σ*	0.01263	2.03	1.17	0.044
C2—S13	σ	1.97473	C3	RY*(1)	0.00644	1.27	1.66	0.041
	σ		C1—C6	σ*	0.02509	3.90	1.23	0.062
	σ		C3—C4	σ*	0.01539	2.08	1.24	0.045
	σ		C7—S14	σ*	0.04531	3.81	0.85	0.051
C3—C4	σ	1.97226	C5	RY*(2)	0.00225	1.53	1.98	0.049
	σ		C2—C3	σ*	0.02077	3.97	1.27	0.063
	σ		C2—S13	σ*	0.02635	5.93	0.90	0.065
	σ		C3—H8	σ*	0.01474	1.12	1.13	0.032
	σ		C4—C5	σ*	0.01574	2.48	1.27	0.050
	σ		C5–H10	σ*	0.01281	2.07	1.15	0.044
C3—C4	π	1.69490	C2	RY*(3)	0.00201	1.12	1.28	0.037
	π		C5	RY*(3)	0.00086	1.76	0.88	0.038
	π		C1—C2	π*	0.47565	18.75	0.27	0.066
	π		C5—C6	π*	0.30984	18.96	0.29	0.066
C3—H8	σ	1.97978	C2	RY*(1)	0.00611	1.32	1.63	0.042
	σ		C4	RY*(1)	0.00610	1.40	1.64	0.043
	σ		C1—C2	σ*	0.04158	4.18	1.06	0.060
	σ		C4—C5	σ*	0.01574	3.56	1.09	0.056
C4—C5	σ	1.97925	C3	RY*(2)	0.00291	1.98	1.84	0.054
	σ		C6	RY*(2)	0.00256	2.05	1.85	0.055
	σ		C3—C4	σ*	0.01539	2.60	1.27	0.051
	σ		C3—H 8	σ*	0.01474	2.46	1.13	0.047
	σ		C5—C6	σ*	0.01340	2.63	1.28	0.052
	σ		C6—H11	σ*	0.01315	2.56	1.14	0.048
C4—H9	σ	1.97949	C3	RY*(1)	0.00644	1.25	1.52	0.039
	σ		C5	RY*(1)	0.00590	1.41	1.61	0.043
	σ		C2—C3	σ*	0.02077	3.66	1.09	0.056
	σ		C5—C6	σ*	0.01340	3.73	1.10	0.057
C5—C6	σ	1.97712	C1	RY*(2)	0.00651	2.09	2.04	0.059
	σ		C4	RY*(2)	0.00219	1.34	1.98	0.046
	σ		C1—C6	σ*	0.02509	2.94	1.27	0.055
	σ		C1—N12	σ*	0.02640	4.71	1.16	0.066
	σ		C4—C5	σ*	0.01574	2.61	1.27	0.051
	σ		C4—H9	σ*	0.01263	2.17	1.15	0.045
	σ		C6—H11	σ*	0.01315	1.16	1.14	0.033
	π	1.69721	C4	RY*(3)	0.00096	1.78	0.78	0.036
	π		C1—C2	π*	0.47565	21.19	0.26	0.070
	π		C3—C4	π*	0.32827	19.72	0.28	0.067

Table 6 (*continued*)

Donor (*i*)	Type	ED/e	Acceptor (*j*)	Type	ED/e	$E^{(2)}$ kcal/mol	$E(j)$–$E(i)$ a.u.	$F(i,j)$ a.u.
C5—H10	σ	1.98018	C4	RY*(1)	0.00610	1.45	1.63	0.044
	σ		C6	RY*(1)	0.00551	1.49	1.79	0.046
	σ		C1—C6	σ*	0.02509	3.56	1.08	0.056
	σ		C3—C4	σ*	0.01539	3.81	1.09	0.058
C6—C11	σ	1.97853	C5	RY*(1)	0.00590	1.13	1.61	0.038
	σ		C1—C2	σ*	0.04158	4.33	1.05	0.061
	σ		C4—C5	σ*	0.01574	3.69	1.09	0.057
C7—N12	σ	1.98906	C1	RY*(1)	0.00742	4.46	2.25	0.089
	σ		C1—C6	σ*	0.02509	3.64	1.47	0.066
	σ		C1—N12	σ*	0.02640	1.75	1.36	0.044
	π	1.90696	C1	RY*(4)	0.00106	1.59	2.00	0.051
	π		S13	RY*(3)	0.00250	1.47	1.02	0.035
	π		S14	RY*(1)	0.00462	1.22	0.85	0.029
	π		C1—C2	π*	0.47565	14.73	0.35	0.072
C7—S13	σ	1.97976	C2—C3	σ*	0.02077	4.34	1.24	0.065
C7—S14	σ	1.98066	C15	RY*(2)	0.00335	1.03	1.56	0.036
	σ		C1—N12	σ*	0.02640	3.64	1.14	0.058
S14—C15	σ	1.97319	C7—S13	σ*	0.08754	3.82	0.76	0.049
	σ		C16—O17	σ*	0.01683	2.53	0.88	0.042
C15—C16	σ	1.99001	O17—H18	σ*	0.00476	1.57	1.07	0.037
C15—H21	σ	1.98463	C16—H19	σ*	0.02885	2.22	0.90	0.040
C15—H22	σ	1.97997	C7—S14	σ*	0.04531	1.31	0.71	0.027
	σ		C16—H20	σ*	0.02487	2.18	0.91	0.040
C16—O17	σ	1.99201	S14—C15	σ*	0.01619	2.40	0.96	0.043
C16—H19	σ	1.98892	C15—H21	σ*	0.01922	2.59	0.92	0.044
C16—H20	σ	1.98746	C15—H22	σ*	0.01374	2.61	0.91	0.043
O17—H18	σ	1.98754	C15—C16	σ*	0.02257	1.88	1.09	0.040
N12	LP(1)	1.87774	C1	RY*(1)	0.00742	3.15	1.53	0.067
	LP (1)		C7	RY*(1)	0.01014	5.24	1.05	0.068
	LP (1)		C1—C2	σ*	0.04158	6.46	0.90	0.069
	LP (1)		C1—C6	σ*	0.02509	1.06	0.93	0.029
	LP (1)		C7—S13	σ*	0.08754	17.06	0.52	0.085
	LP(1)		C7—S14	σ*	0.04531	2.13	0.55	0.031
S13	LP (1)	1.98215	C2	RY*(1)	0.00611	1.68	1.77	0.049
	LP(1)		C7	RY*(1)	0.01014	1.02	1.36	0.033
	LP(1)		C1—C2	σ*	0.04158	1.55	1.21	0.039
	LP(1)		C7—N12	σ*	0.02500	3.48	1.24	0.059
	LP(2)	1.69143	C1—C2	π*	0.47565	17.73	0.27	0.064
	LP(2)		C7—N12	π*	0.38845	26.29	0.24	0.072
S14	LP(1)	1.97878	C7—N12	σ*	0.02500	6.21	1.21	0.078
	LP(2)	1.80916	C7—N12	π*	0.38845	27.82	0.23	0.075
	LP(2)		C15—C16	σ*	0.02257	4.08	0.62	0.047
	LP(2)		C15—H21	σ*	0.01922	1.97	0.66	0.034
	LP(2)		C16—O17	σ*	0.01683	1.18	0.53	0.023
O17	LP(1)	1.98317	C16	RY*(2)	0.00300	2.85	1.64	0.061
	LP(1)		H18	RY*(2)	0.00145	1.55	2.22	0.053
	LP(1)		C16—H20	σ*	0.02487	1.26	1.01	0.032
	LP(2)	1.96060	C16	RY*(4)	0.00181	1.19	1.83	0.042
	LP(2)		H18	RY*(1)	0.00179	2.20	1.84	0.057
	LP(2)		C16—H19	σ*	0.02885	7.69	0.69	0.065
	LP(2)		C16—H20	σ*	0.02487	4.27	0.70	0.049
C1—C2	π*	1.63698	C1	RY*(5)	0.00106	2.13	1.03	0.086
	π*		S13	RY*(1)	0.00391	1.09	0.62	0.047
	π*		C3—C4	π*	0.32827	184.98	0.02	0.084
	π*		C5—C6	π*	0.30984	154.96	0.02	0.084
C3—C4	π*	1.69490	C4	RY*(3)	0.00096	1.65	0.50	0.063
C5—C6	π*	1.69721	C6	RY*(3)	0.00078	2.96	0.46	0.084
C7—N12	π*	1.90696	C7	RY*(3)	0.00532	2.61	1.09	0.107
	π*		N12	RY*(2)	0.00258	1.44	0.69	0.064
	π*		N12	RY*(4)	0.00193	1.03	0.83	0.059
	π*		C1—C2	π*	0.47565	87.02	0.03	0.070

23.8566×10^{-24} esu and 6.6139×10^{-30} esu, respectively. The total first static hyperpolarizability (β_{total}) of BTZTE nearly 34 times more than β_{total} of urea (0.1947×10^{-30} esu) indicates that BTZTE molecule possesses nonlinear optical properties and is a potential candidate for nonlinear optical applications.

NBO analysis

The NBO studies a basic for exploring charge transfer or conjugative interaction in molecular systems and is an efficient method to know about intra- and intermolecular bonding and interaction among bonds. The NBO analysis were performed on the molecule and summary of electron donor orbital, acceptor orbital and the interaction stabilization energy that resulted from the second-order perturbation theory is reported in Table 6. The larger value of $E^{(2)}$ gives the stronger interaction between electron donors (i) and electron acceptor (j) and reflects a more donating tendency from electron donor to electron acceptor and consequently a greater degree of conjugation of the whole system. Delocalisation of the electron density between occupied Lewis-type (bond or lone

pair) NBO orbital and formally unoccupied (antibond and Rydgberg) non Lewis NBO orbital, corresponds to a stabilizing donor acceptor interaction. Table 6 shows that in the title molecule the intra-molecular interactions are due to the orbital overlap between bonding π (C—C) to π^* (C—C); π (C7—N12) to π^* (C1—C2); LP1 (N12) to σ^* (C7—S13); LP2 (S13) to π^* (C1—C2) and π^* (C7—N12); LP2 (S14) to π^* (C7—N12). The interaction energy related to the resonance in the title molecule involves electron density from lone pair (2) of S13 and S14 to antibonding π^* of (C7—N12) leads to the enormous stabilization (up to 27.82 kcal/mol). In Table S1, the direction of the line of centre between the two nuclei is compared with the hybrid direction to determine the bending of the bond, expressed as the deviation angle between these two directions. The hybrid directionality and bond bending analysis of natural hybrid orbitals (NHOs) provides a clue of the substituent effect and steric effect. The bending of S13 from the line of C7—S13 centre is more than the bending of S14 from the line of C7—S14 centre. It is pointed out that the stabilization energy corresponding to the overlap between LP(2) of S14 with π^* (C7—N12) is slightly higher than the corresponding overlap of LP(2) of S13, the strong intermolecular hyper conjugation of π (C1—C2) to antibonding π^* (C3—C4) and π^* (C5—C6) lead to stabilization of 19.59 kcal/mol and 16.30 kcal/mol respectively.

NMR studies

Recent advances in experimental and computational techniques have made it possible to exploit NMR chemical shifts to obtain structure of proteins and macromolecules [40,41]. The optimized structure of BTZTE was used to calculate the NMR spectrum at the B3LYP/6-311++G(d,p) level using the GIAO method in which an exponential term containing the vector potential is included with each atomic orbital. The recorded ^{1}H NMR spectrum in DMSO-d_6 solution is given in Fig. 6 and the calculated chemical shifts along with experimental signal values are collected in Table 7. The studied molecule has nine hydrogen atoms, four attached to phenyl ring and five as a part of ethanol. In theoretical ^{1}H NMR spectrum, the chemical shift values lie in the range of 7.88–7.35 ppm (with respect to TMS) and experimental signal in the range of 7.98–7.34 ppm. The chemical shifts of ethanol group are calculated in the range of 4.27–2.80 ppm in DMSO while the experimental signals are observed in the range of 3.77–2.50 ppm. The singlet signal at 5.15 ppm is assigned due resonance of H18 atom, this downfield shifting is due to attached electronegative O atom. The discrepancy between the theoretical and observed values is may be due to the strong intermolecular hydrogen bonding O—H. . .. . .O present in system.

Table 7
The observed (in DMSO) and calculated isotropic chemical shifts.

Atom	Exp.	6-311++G(d,p)		6-311++G(d,p)		
		Gas	DMSO	Atom	Gas	DMSO
H(8)	7.84	7.54	7.88	C(1)	153.3	153.6
H(9)	7.34	7.05	7.35	C(2)	143.0	143.4
H(10)	7.45	7.15	7.43	C(3)	120.7	122.5
H(11)	7.98	7.70	7.88	C(4)	124.0	125.4
H(18)	5.15	0.06	0.92	C(5)	125.8	127.1
H(19)	3.47	3.50	3.70	C(6)	122.4	122.5
H(20)	3.77	4.17	4.27	C(7)	176.7	178.8
H(21)	3.57	3.89	3.84	C(15)	35.1	35.8
H(22)	2.50	2.57	2.80	C(16)	61.3	61.8

Global and local reactivity descriptors

The global reactivity descriptors like chemical potential, electronegativity, hardness, softness, and electrophilicity index and local reactivity descriptor like Fukui functions can be defined within the scaffold of DFT. Following Parr and Pearson [42], the electronic chemical potential, describing the escaping tendency of electrons from a stable system can be calculated as $\mu = -(IP + EA)/2$. Electronegativity (χ) is defined as negative of the electronic chemical potential. Chemical hardness, given by $\eta = (IP - EA)/2$, enumerates the resistance to alteration in electron distribution and is correlated with the stability and reactivity of a chemical system. The inverse of the hardness is expressed as the global softness $S = 1/\eta$. The global electrophilicity index (ω), introduced by Parr et al. [42] is calculated in terms of the chemical potential and the hardness as $\omega = \mu^2/2\eta$ and assess the lowering of energy due to maximal electron flow between donor and acceptor. Here the ionization potential (IP) and electron affinity (EA) are defined as the difference in the ground state energy between the cationic and neutral system and difference in the ground state energy between neutral and anionic system i.e. IP = E(N − 1)–E(N) and EA = E(N)−E(N + 1). The global reactivity descriptors for BTZTE are listed in Table S2 of supplementary material.

Condensed Fukui functions (f_k) which are most frequently used local reactivity descriptor were calculated using NBO population schemes. The equations governing nucleophilic, electrophilic and radical attack are $f_k^+ = [q(N+1) - q(N)]$, $f_k^- = [q(N) - q(N-1)]$ and $f_k^0 = 1/2[q(N+1) - q(N-1)]$ respectively [43]. The natural atomic charges were calculated using NBO population analysis at B3LYP/6-311++G(d,p) level of theory. The comparative graphical view of the calculated Fukui functions given in Fig. S2 (Table S3 of supplementary material) show the reactivity order for

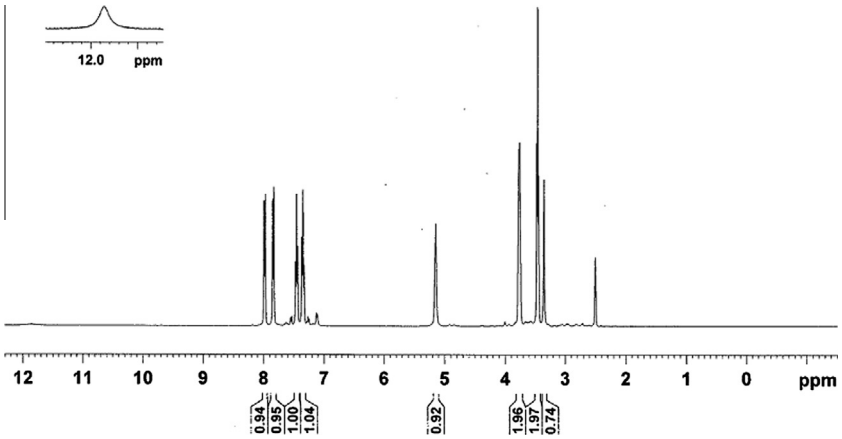

Fig. 6. Recorded ^{1}H NMR spectrum of BTZTE in DMSO solvent showing chemical shift with respect to TMS.

electrophilic attack to be S14 > C4 > S13 > C1 > N12 > C5 and predict that the most preferred sites on BTZTE molecule for nucleophilic attack are H18 and C7.

Thermodynamical analysis

On the basis of vibrational analysis, the statistical thermodynamic functions: heat capacity ($C^0_{p,m}$) entropy (S^0_m) and enthalpy changes (ΔH^0_m) at different temperatures (100–700 K) along with Zero point vibrational energy (102.82904 kcal/mol) and rotational constants at standard temperature and pressure (298.15 K and 1 atm) for the title compound were obtained using DFT-B3LYP/6-311++G(d,p) method and listed in Table S4 of supplementary material. The correlation between these thermodynamic properties and temperatures shown in Fig. S3 predict that values of heat capacity, entropy and enthalpy increases with the increase of temperature from 100 K to 700 K, which is attributed to the enhancement of molecular vibrational intensities with the temperature. The correlation equations between heat capacity, entropy, enthalpy changes and temperatures were fitted by quadratic formulas and the corresponding fitting factors (R^2) for these thermodynamic properties are 0.9994, 0.9999 and 0.9999, respectively. The corresponding fitting equations are as follows

$$(C^0_{p,m}) = 3.5267 + 0.165T - 7 \times 10^{-5}T^2 \quad (R^2 = 0.9994)$$

$$(S^0_m) = 58.438 + 0.1997T - 6 \times 10^{-5}T^2 \quad (R^2 = 0.9999)$$

$$(\Delta H^0_m) = -0.6659 + 0.0145T - 5 \times 10^{-5}T^2 \quad (R^2 = 0.9999)$$

All the thermodynamic data may deliver useful information for the further study on BTZTE compound. These parameters are useful in Thermo-chemical field as they can be used to compute the other thermodynamic energies and estimate directions of chemical reactions according to relationships of thermodynamic functions and using second law of thermodynamics. [44].

Conclusions

In this study, we carried out the experimental and theoretical spectroscopic analysis of BTZTE for the first time. In the optimized structure of BTZTE, S14 and C15 atoms of ethanol group are almost planer with the bicyclic ring and the C(16)H_2 group is almost perpendicular to the plane of the ring. The modes of vibrations were explicitly assigned using the recorded vibrational spectra and results of TED obtained from the normal coordinate analysis. The mean polarizability and total first static hyperpolarizability (β_{total}) of the molecule is found to be 23.8566×10^{-24} esu and 6.6139×10^{-30} esu, respectively. The β_{total} value of BTZTE nearly 34 times more than β_{total} of urea (0.1947×10^{-30} esu) indicates that BTZTE molecule possesses nonlinear optical properties and is a potential candidate for nonlinear optical applications. The calculated fukui functions show the reactivity order for electrophilic attack to be S14 > C4 > S13 > C1 > N12 > C5 and predict that the most preferred sites on BTZTE molecule for nucleophilic attack are H18 and C7.

Acknowledgements

The authors are thankful to Sophisticated Analytical Instrumentation Facility (SAIF), Central Drug Research Institute, Lucknow, India for providing FT-IR and UV spectral measurements and AIRF, Jawaharlal Nehru University, New Delhi for giving permission to use Raman Spectrometer for getting recorded the laser Raman spectrum. S. K. Pathak is grateful to the University Grants Commission (UGC), New Delhi, India for the financial assistance as JRF.

Appendix A. Supplementary material

Supplementary data associated with this article can be found, in the online version, at http://dx.doi.org/10.1016/j.saa.2014.09.091.

References

[1] H.D. Wever, H. Verachtert, Wat. Res. 31 (11) (1997) 2673–2684.
[2] Y. Zhang, R.Z. Qiao, C.F. Dai, P.F. Xu, Z.Y. Zhang, Chin. Chem. Lett. 13 (4) (2002) 287–289.
[3] N. Siddiqui, A. Rana, S.A. Khan, Indian J. Pharm. 69 (1) (2007) 10–17.
[4] A.R. Katritzky, C.W. Rees, J.V. Metzyer, Comprehensive heterocyclic chem. Oxford, 1996.
[5] G. Wells, T.D. Bradshaw, P. Diana, A. Seaton, D.F. Shi, A.D. Westwell, M.F. Stevens, Bioorg. Med. Chem. Lett. 10 (2000) 513–515.
[6] I. Hutchinson, M.S. Chua, H.L. Browne, V. Trapani, T.D. Bradshaw, A.D. Westwell, M.F. Stevens, J. Med. Chem. 44 (2001) 1445–1446.
[7] I. Hutchinson, S.A. Jennings, B.R. Vishnuvajjala, A.D. Westwell, M.F. Stevens, J. Med. Chem. 45 (2002) 744–747.
[8] C.D. Hose, M. Hollingshead, E.A. Sausville, A. Monks, Mol. Cancer Ther. 2 (2003) 1265–1272.
[9] S. Saeed, N. Rashid, P.G. Jones, M. Ali, R. Hussain, Eur. J. Med. Chem. 45 (2010) 1323–1331.
[10] S.J. Tangeda, A. Garlapati, Eur. J. Med. Chem. 45 (2010) 1453–1458.
[11] V.R. Solomon, C. Hu, H. Lee, Bioorg. Med. Chem. 17 (2009) 7585–7592.
[12] L. Sinha, O. Prasad, M. Karabacak, H.N. Mishra, V. Narayan, A.M. Asiri, Spectrochim. Acta A 120 (2014) 126–136.
[13] A.D. Becke, J. Chem. Phys. 98 (1993) 5648–5652.
[14] C. Lee, W. Yang, R.G. Parr, Phys. Rev. B37 (1998) 785–789.
[15] B. Miehlich, A. Savin, H. Stoll, H. Preuss, Chem. Phys. Lett. 157 (1989) 200–206.
[16] W. Kohn, L.J. Sham, Phys. Rev. A 140 (1965) 1133–1138.
[17] J.B. Foresman, A. Frisch, Exploring Chemistry with Electronic Structure Methods, second ed., Gaussian Inc., Pittushburg, PA, 1996.
[18] J. Baker, A.A. Jarzecki, P. Pulay, J. Phys. Chem. 102 (1998) 1412–1424.
[19] A. Frisch, H.P. Hratchian, R.D. Dennington, T.A. Keith, J. Millam, B. Nielsen, A.J. Holder, J. Hiscocks, GaussViewVersion 5.0.8, Gaussian Inc, Wallingford, CT, USA, 2009.
[20] SQM version 1.0, Scaled Quantum Mechanical Force Field, 2013 Green Acres Road, Fayetteville, Arkansas 72703.
[21] G. Keresztury, S. Holly, J. Varga, G. Besenyei, A.Y. Wang, J.R. Durig, Spectrochim. Acta 49 (1993) 2007–2017.
[22] G. Keresztury, Raman spectroscopy: theory, in: J.M. Chalmers, P.R. Griffith (Eds.), Handbook of Vibrational Spectroscopy, Vol. 1, John Wiley & Sons, New York, 2002.
[23] D.A. Kleinman, Phys. Rev. 126 (1962) 1977–1979.
[24] J. Pipek, P.G. Mezey, J. Chem. Phys. 90 (1989) 4916–4926.
[25] A.D. Buckingham, Adv. Chem. Phys. 12 (1967) 107–142.
[26] E.D. Glendening, C.R. Landis, F. Weinhold, WIREs Comput. Mol. Sci, John Wiley & Sons, Ltd., 2011. p. 1–42.
[27] R. Ditchfield, J. Chem. Phys. 56 (11) (1972) 5688–5691.
[28] K. Wolinski, J.F. Hinton, P. Pulay, J. Am. Chem. Soc. 112 (23) (1990) 8251–8260.
[29] G. Varsanyi, Assignments for Vibrational Spectra of Seven Hundred Benzene Derivatives, vol. 1–2, Academic Kiaclo, Budapest, 1973.
[30] M. Cinar, A. Coruh, M. Karabacak, Spectrochim. Acta A 83 (2011) 561–569.
[31] Y. Wang, S. Saebo, C.U. Pittman, J. Mol. Struct. (Theochem) 281 (1993) 91–98.
[32] M. Karabacak, M. Cinar, M. Kurt, Spectrochim. Acta A 74 (2009) 1197–1203.
[33] A. Altun, K. Golcuk, M. Kumru, J. Mol. Struct. (Theochem) 637 (2003) 155–169.
[34] R.M. Silverstein, F.X. Webster, D. Kiemle, Spectrometric Identification of Organic Compounds, seventh ed., Jon-Wiley & Sons Inc, 2005.
[35] M. Karabacak, M. Cinar, M. Kurt, J. Mol. Struct. 968 (2010) 108–114.
[36] M. Jag, Organic Spectroscopy-Principles and Applications, second ed. New Delhi 2001.
[37] M. Karabacak, Z. Cinar, M. Kurt, S. Sudha, N. Sundaraganesan, Spectrochim. Acta A 85 (2012) 179–189.
[38] L.J. Bellamy, The Infrared Spectra of Complex Molecules, Chapman and Hall, London, 1980.
[39] A. Coruh, F. Yilmaz, B. Sengez, M. Kurt, M. Cinar, M. Karabacak, Struct. Chem. 22 (2011) 45–56.
[40] T. Schlick, Molecular Modeling and Simulation: An Interdisciplinary Guide, vol. 21, Springer, New York, 2010. second ed..
[41] A. Cavalli, X. Salvatella, C.M. Dobson, M. Vendruscolo, Proc. Natl. Acad. Sci. USA 104 (2007) 9615–9620.
[42] R.G. Parr, R.G. Pearson, J. Am. Chem. Soc. 105 (1983) 7512–7516.
[43] P.W. Ayers, M. Levy, Theor. Chem. Acc. 103 (2000) 353–360.
[44] J. Bevan Ott, J. Boerio-Goates, Calculations from Statistical Thermodynamics, Academic Press, 2000.